

Magnetic form factor analysis on detwinned single crystal of BaFe₂As₂

K. Kodama,¹ M. Ishikado,² S. Wakimoto,¹ K. Kihou,³ C. H. Lee,³ A. Iyo,³ H. Eisaki,³ and S. Shamoto¹

¹Quantum Beam Science Center, Japan Atomic Energy Agency, Tokai, Ibaraki 319-1195, Japan

²Comprehensive Research Organization for Science and Society (CROSS), Tokai, Ibaraki 319-1106, Japan

³Nanoelectronics Research Institute, National Institute of Advanced Industrial Science and Technology, Tsukuba, Ibaraki 305-8562, Japan

(Dated: April 16, 2021)

We have performed neutron diffraction measurement on a single crystal of parent compound of iron-based superconductor, BaFe₂As₂ at 12 K. In order to investigate in-plane anisotropy of magnetic form factor in the antiferromagnetic phase, the detwinned single crystal is used in the measurement. The magnetic structure factor and magnetic form factor are well explained by the spin densities consisting of $3d_{yz}$ electrons with a fraction of about 40 % and the electrons in the other four $3d$ orbitals with each fraction of about 15 %. Such anisotropic magnetic form factor is qualitatively consistent with the anisotropic magnetic behaviors observed in the antiferromagnetic phase of the parent compound of iron-based superconductor.

PACS numbers: 74.70.Xa, 75.25.-j, 75.50.Ee, 75.30.Gw

In-plane anisotropy observed in electronic properties of iron-based superconductors is one of the important issues in relation to the mechanism of the superconductivity. The parent compound of the iron-based superconductor exhibits structural phase transition from tetragonal to orthorhombic structures with decreasing temperature, whereas the superconducting phase achieved by partial atomic substitution remains tetragonal structure down to the lowest temperature. In the superconducting phase and the tetragonal phase of the parent compound, the electronic properties exhibit two-fold symmetry in FeAs layer although the crystal structure is the tetragonal with four-fold symmetry.¹ Such in-plane anisotropy which is so-called nematic state probably originate from degrees of freedom of electrons. So-called spin nematic state and the orbital ordering are suggested as the origin of the strong breaking of four-fold symmetry.²⁻⁶

In the orthorhombic phases of a parent compound and non-superconducting underdoped compounds, the clear in-plane anisotropy has been observed in both of the electronic and magnetic properties. Electric resistivity along b -direction is about twice larger than the resistivity along a -direction in the orthorhombic phase of underdoped Ba(Fe_{1-x}Co_x)₂As₂.^{7,8} Optical conductivity below about 0.2 cm^{-1} along a -direction is also about twice larger than the conductivity along b -direction in BaFe₂As₂.^{9,10} Drastic change of Fermi surfaces with from fourfold symmetry to that with twofold symmetry is observed below the antiferromagnetic transition temperature due to resolving a degeneracy between $3d_{yz}$ and $3d_{zx}$ orbitals.¹¹ The energy dispersion of the spin wave in the antiferromagnetic phase observed by inelastic neutron scattering has large anisotropy which is explained by considering the nearest neighboring magnetic interactions along a and b directions with opposite sign.¹²⁻¹⁴ These anisotropic behaviors observed in the orthorhombic phase are more pronounced than that simply expected from the small difference between a and b lattice constants (less than 1 %). These results suggest that the electronic state,

for example, the spatial distribution of the $3d$ electrons which contribute to the electronic and magnetic properties is largely anisotropic. However, early neutron diffraction measurement on a single crystal sample of the parent compound including twinned domains has reported that the magnetic form factor which is estimated from magnetic Bragg intensities of $h0l$ reflections is almost isotropic,¹⁵ inconsistent with the above anisotropic magnetic behaviors. In this letter, results of neutron diffraction measurement on a detwinned single crystal of BaFe₂As₂ in the antiferromagnetic phase are reported. The magnetic form factor determined from the magnetic Bragg intensities of both of hkh and $h0l$ reflections is anisotropic in a - b plane, qualitatively consistent with the anisotropic magnetic behaviors.

A single crystal of BaFe₂As₂ was grown by self-flux method. The details are reported in ref. 16. The crystal with a volume of $4 \times 4 \times 0.5 \text{ mm}^3$ was used in neutron diffraction measurement. The neutron diffraction measurement was performed using the triple-axis spectrometer TAS-1 installed at the research reactor JRR-3 of Japan Atomic Energy Agency. The single crystal was detwinned in a sample holder made of Al by uniaxial pressure along b -axis in the orthorhombic phase. In the estimations of nuclear and magnetic Bragg intensities, the neutron absorption of the sample folder is corrected by considering the neutron flight paths in the sample folder for each Bragg reflections. The sample was sealed in an aluminum can, and then mounted in a closed-cycle He gas refrigerator. Collimation sequence of open-open-S-80'-open (S denotes sample) were used. Pyrolytic graphites (PGs) were used as a monochromator and an analyzer. Another PG was placed downstream of the sample to eliminate higher order neutrons. The detwinning was confirmed at 12 K by $\theta - 2\theta$ scan with the neutron wave length of 2.3532 \AA , as shown in Fig. 1. The nuclear and magnetic Bragg reflections were collected by $\theta - 2\theta$ scan with the neutron wave length of 1.6377 \AA . The crystal was oriented with two types of configurations including

the reciprocal lattice points of hkh and $h0l$ in the horizontal scattering planes.

Figures 1(a) and 1(b) show the profiles of 040 and 400 nuclear Bragg reflections obtained in the conditions to collect the intensity of hkh and $h0l$ reflections, respectively. The data are collected at room temperature and 12 K where the crystal structures are tetragonal and orthorhombic, respectively. Here, because we use the notation of the orthorhombic structure, the reflections at room temperature correspond with 220 reflection in the tetragonal structure. The peak width at room tempera-

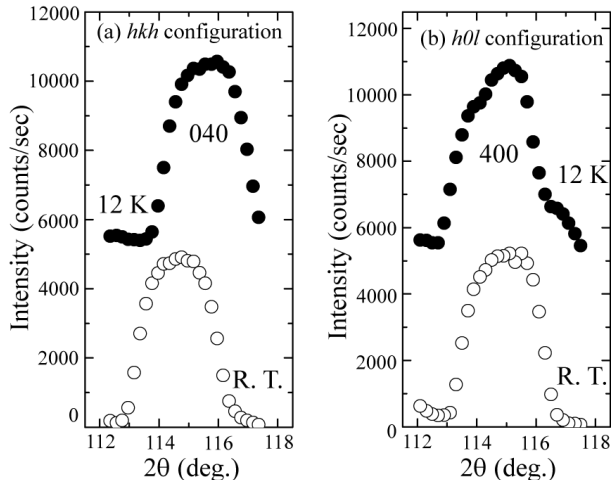


FIG. 1: Peak profiles of 040 (a) and 400 (b) nuclear Bragg reflections obtained in the scattering conditions to collect the intensity of hkh and $h0l$ reflections, respectively. The data are collected at 12 K (closed circles) and room temperature (open circles).

ture almost corresponds with the instrumental resolution (momentum transfer of about 0.1 \AA^{-1} in the condition with the neutron wave length of 2.3532 \AA). 040 and 400 reflections of the orthorhombic phase at 12 K are observed at different positions and their peak widths almost correspond with the width at room temperature, indicating that the detwinned single crystal is obtained at 12 K. The lattice constants at 12 K estimated from the positions of the peak centers of 400, 040 and 002 reflections are $a = 5.601 \text{ \AA}$, $b = 5.568 \text{ \AA}$ and $c = 12.95 \text{ \AA}$, respectively. In Fig. 2, the observed nuclear structure factor squared, $|F_N|_{obs}^2$, is plotted against the calculated structure factor squared, $|F_N|_{cal}^2$. The observed data are corrected by Lorentz factor, $L(\theta)$. Here, we use the atomic positions reported for the orthorhombic phase in the calculation of $|F_N|_{cal}^2$.¹⁷ The solid line is the fitting result by using a formula $|F_N|_{obs}^2 = A|F_N|_{cal}^2(1 - B|F_N|_{cal}^2)$, where A is a scale factor and B accounts for extinction.¹⁸

By using the scale factor A determined from the analysis on nuclear Bragg intensities, the intensities of magnetic Bragg reflections are described by using following

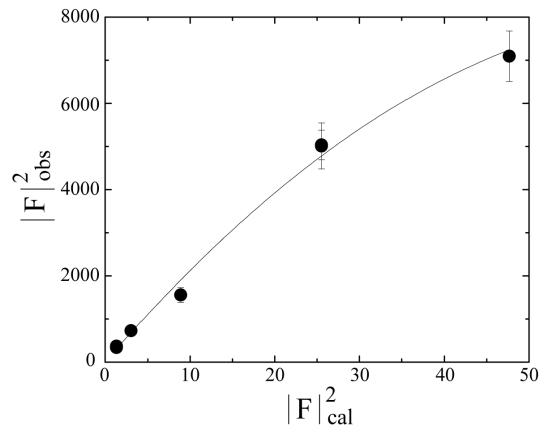


FIG. 2: Observed nuclear structure factor squared, $|F_N|_{obs}^2$, is plotted against squared nuclear structure factor $|F_N|_{cal}^2$ calculated by using the atomic positions reported in ref. 17. Solid line is fitting result by using a formula $|F_N|_{obs}^2 = A|F_N|_{cal}^2(1 - B|F_N|_{cal}^2)$.

equations.

$$I_{obs}(\mathbf{Q}) = A \times L(\theta) |F|_{obs}^2, \quad (1)$$

$$|F|_{obs}^2 = \gamma_0^2 \mu^2 f_{obs}(\mathbf{Q})^2 \times \left| \sum_n \sin \alpha_n \exp[(2\pi i)(hx_n + ky_n + lz_n)] \right|^2 \quad (2)$$

$$L(\theta) = 1/\sin 2\theta, \quad (3)$$

where the summation is taken over all magnetic moment in the magnetic unit cell and $\gamma_0 = 0.269 \times 10^{-12} \text{ cm}$, μ is the amplitude of ordered magnetic moment in the unit of Bohr magneton, and α is the angle between the direction of n -th magnetic moment and the scattering vector \mathbf{Q} . The magnetic structure in the antiferromagnetic phase has already been reported, as schematically shown in Fig. 3(a).¹⁹⁻²¹ The magnetic moments have antiferromagnetic and ferromagnetic arrangements along a - and b -directions, respectively, and are almost parallel to a -direction, which is so-called stripe type magnetic structure. For this magnetic structure, the magnetic reflection is observed at hkl with $h = 2n + 1$, $k = 2n$ and $l = 2n + 1$, where n is an integer. If we assume that the direction of the magnetic moment is slightly away from a -axis in a - b plane, ϕ , as shown in Fig. 3(a), the magnetic structure factor depend on ϕ and eq. (2) can be rewritten as follows.

$$|F|_{obs}^2 = 64\gamma_0^2\mu^2 f_{obs}(\mathbf{Q})^2 \times \left| \sin \left\{ \cos^{-1} \left(\frac{ha^* \cos \phi + kb^* \sin \phi}{Q\mu} \right) \right\} \right|^2. \quad (4)$$

Although the observed magnetic structure factor squared, $|F|_{obs}^2$, and the observed magnetic form factor, $f_{obs}(\mathbf{Q})$, can be determined from the observed magnetic Bragg intensities and the equations (1), (3) and (4), the

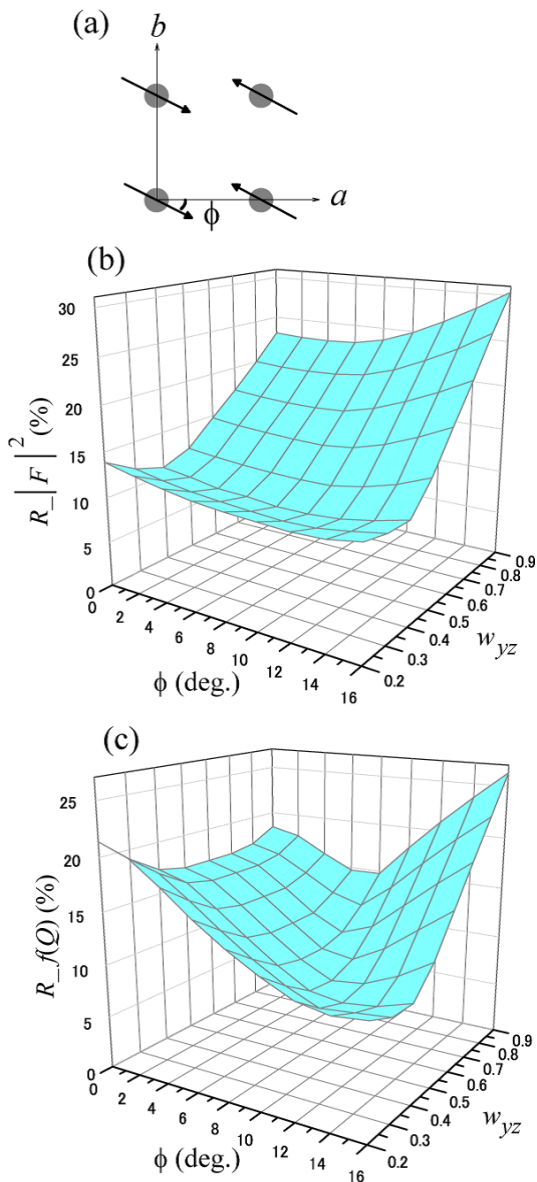


FIG. 3: (Color online) (a) Magnetic structure in antiferromagnetic phase of BaFe_2As_2 . R -factors estimated from $|F|_{obs}^2$ and $|F|_{cal}^2$ (b), and those from $f_{obs}(\mathbf{Q})$ and $f_{cal}(\mathbf{Q})$ (c), are plotted against ϕ and w_{yz} .

estimated value of the latter depends on ϕ . Here, we compare the $|F|_{obs}^2$ and $f_{obs}(\mathbf{Q})$ with the calculated magnetic structure factor squared, $|F|_{cal}^2$, and magnetic form factor, $f_{cal}(\mathbf{Q})$, which are obtained by following equations.

$$|F|_{cal}^2 = 64\gamma_0^2\mu^2 f_{cal}(\mathbf{Q})^2 \times \left| \sin \left\{ \cos^{-1} \left(\frac{ha^* \cos \phi + kb^* \sin \phi}{Q\mu} \right) \right\} \right|^2, \quad (5)$$

$$f_{cal}(\mathbf{Q}) = w_{yz}f_{yz}(\mathbf{Q}) + \frac{1-w_{yz}}{4} \times \{f_{xy}(\mathbf{Q}) + f_{zx}(\mathbf{Q}) + f_{x^2-y^2}(\mathbf{Q}) + f_{3z^2-r^2}(\mathbf{Q})\} \quad (6)$$

Here, x , y , and z directions correspond with a , b , and

c directions of the orthorhombic lattice, respectively. Although the isotropic magnetic form factor has been reported,¹⁵ we consider the anisotropic one which has larger weight of the $3d_{yz}$ orbital than the other orbitals because the ferro-orbital ordering model in which the electrons in $3d_{yz}$ orbital has large contribution to the magnetic moment is suggested.⁵ In the calculations of above equations, the form factors and the wave functions of $3d$ orbitals reported on Fe ion are used.²²⁻²⁴

Figures 3(b) and 3(c) show R -factors estimated from $|F|_{obs}^2$ and $|F|_{cal}^2$, and from $f_{obs}(\mathbf{Q})$ and $f_{cal}(\mathbf{Q})$, for various ϕ and w_{yz} , respectively. They are estimated by following equations.

$$R = \frac{\sum_i |W_i^{obs} - W_i^{cal}|}{\sum_i W_i^{obs}}, \quad (7)$$

where W_i^{obs} and W_i^{cal} are observed and calculated values of the squared magnetic structure factors and magnetic form factors. \sum_i means a summation taken over all observed magnetic Bragg reflections. The R -factor has minimum value of 9.4 % at $\phi=10$ deg. and $w_{yz} = 0.4$ for the squared magnetic structure factor, and the R -factor for the magnetic form factor has minimum value of 8.0 % at $\phi=12$ deg. and $w_{yz} = 0.4$. The values of ϕ and w_{yz} where the R obtained from $|F|_{obs}^2$ and $|F|_{cal}^2$ is minimum, is almost consistent with the values where the R obtained from $f_{obs}(\mathbf{Q})$ and $f_{cal}(\mathbf{Q})$ is minimum. The weight of $3d_{yz}$ orbital is larger than the each weight of the other $3d$ orbitals (w_{yz} is about 0.4 and the other weights are about 0.15). They indicate that the such anisotropic magnetic form factor must be considered to reproduce the observed magnetic structure factor and magnetic form factor. In Figs. 4(a) and 4(b), $|F|_{obs}^2$ and $f_{obs}(\mathbf{Q})$ are plotted against $|F|_{cal}^2$ and $f_{cal}(\mathbf{Q})$, respectively. The plotted values are obtained for $\phi=10$ deg. and $w_{yz} = 0.4$. Here, we adopt the amplitude of magnetic moment, $\mu = 0.70\mu_B$, optimized in the above analysis. The observed values are almost reproduced by the calculated values, and the weighted R factors are 9.4 % and 8.4 % for the squared magnetic structure factor and the magnetic form factor, respectively. In Fig. 4(c), Q -dependences of the observed magnetic form factors at $h01$, $1k1$, $h03$, and $10l$ reflections estimated by using above ϕ , w_{yz} and μ values, are shown by closed circles, small open circles, closed triangles and large open circles, respectively. The Q -dependence of $f_{obs}(\mathbf{Q})$ at $1k1$ almost correspond with that of $10l$ reflections. The decreases with Q of $f_{obs}(\mathbf{Q})$ at $h01$ and $h03$ reflections are more gradual than those at $1k1$ and $10l$ reflections. The lines which show the magnetic form factors calculated for above reciprocal lattice points, almost reproduce the $f_{obs}(\mathbf{Q})$. From these analyses, we know that the magnetic form factor has in-plane anisotropy.

The early neutron diffraction study on SrFe_2As_2 has claimed that magnetic form factor is approximately isotropic,¹⁵ inconsistent with our result. In their data, the magnetic form factor at 501 reflection is zero. We

speculate that clear magnetic Bragg peak of the 501 reflection can not be detected in their experimental accuracy because the structure factor of the 501 reflection is much smaller than the intensities at the reciprocal lattice points with larger l values. If the 501 reflection can be detected, their magnetic form factor must have similar in-plane anisotropy to our result, because the decrease with Q of the magnetic form factor at $h01$ with $h=1$ and 3 is also slower than that at the other reciprocal lattice points, for example, $10l$ in their data.

The orbital ordering model in which the electrons in half-filled $3d_{yz}$ orbital mainly gives the magnetic moment and the electrons in fully filled $3d_{zx}$ orbital is non-magnetic, is suggested.⁵ In such orbital ordering state, the antiferromagnetic magnetic interaction along a axis is much larger than the interaction along b axis, reproducing the stripe type magnetic structure and the large anisotropy of the spin wave dispersion. Schematic spin density expected from obtained magnetic form factor is shown in Fig. 4(d). The spin density is qualitatively

consistent with the orbital ordering model although it is moderate relative to the above model. Our result can lead to the understanding the in-plane anisotropy of the magnetic behaviors.

In summary, the magnetic structure factor and the magnetic form factor which are determined by the neutron diffraction measurement on a detwinned single crystal of BaFe_2As_2 can be explained by considering that about half of the magnetic moment are contributed from the electrons in $3d_{yz}$ orbital. Such anisotropic spin density in a - b plane is qualitatively consistent with the in-plane anisotropy of the magnetic behaviors observed in the antiferromagnetic phase of the parent compounds of the iron based superconductors.

This work was supported by a Grant-in-Aid for Specially Promoted Research 17001001 from the Ministry of Education, Culture, Sports, Science and Technology, Japan, and JST TRIP. This work was supported by a Grant-in-Aid for Scientific Research B (No. 24340090) from the Japan Society for the Promotion of Science.

-
- ¹ S. Kasahara, H. J. Shi, K. Hashimoto, S. Tonegawa, Y. Mizukami, T. Shibauchi, K. Sugimoto, T. Fukuda, T. Terashima, A. H. Nevidomskyy, and Y. Matsuda, *Nature* **486** 382 (2012).
- ² R. M. Fernandes, A. V. Chubukov, J. Knolle, I. Eremin, and J. Schmalian, *Phys. Rev. B* **85** 024534 (2012).
- ³ F. Krüger, S. Kumar, J. Zaanen, and J. vandenBrink, *Phys. Rev. B* **79** 054504 (2009).
- ⁴ W. Lv, J. Wu, and P. Phillips, *Phys. Rev. B* **80** 224506 (2009).
- ⁵ C. C. Lee, W.-G. Yin, and W. Ku, *Phys. Rev. Lett.* **103** 267001 (2009).
- ⁶ R.M. Fernandes, A. V. Chubukov, and J. Schmalian, *Nature Phys.* **10** 97 (2014).
- ⁷ J.-H. Chu, J. G. Analytis, K. D. Greve, P. L. McMahon, Z. Islam, Y. Yamamoto, and I. R. Fisher, *Science* **329** 824 (2010).
- ⁸ S. Ishida, M. Nakajima, T. Liang, K. Kihou, C. H. Lee, A. Iyo, H. Eisaki, T. Kakeshita, Y. Tomioka, T. Ito, and S. Uchida, *Phys. Rev. Lett.* **110** 207001 (2013).
- ⁹ M. Nakajima, T. Liang, S. Ishida, Y. Tomioka, K. Kihou, C. H. Lee, A. Iyo, H. Eisaki, T. Kakeshita, T. Ito, and S. Uchida, *Proc. Natl. Acad. Sci. U.S.A.* **108** 12238 (2011).
- ¹⁰ M. Nakajima, S. Ishida, Y. Tomioka, K. Kihou, C. H. Lee, A. Iyo, T. Ito, T. Kakeshita, H. Eisaki, and S. Uchida, *Phys. Rev. Lett.* **109** 217003 (2012).
- ¹¹ T. Shimojima, K. Ishizaka, Y. Ishida, N. Katayama, K. Ohgushi, T. Kiss, M. Okawa, T. Togashi, X.-Y. Wang, C.-T. Chen, S. Watanabe, R. Kadota, T. Oguchi, A. Chainani, and S. Shin, *Phys. Rev. Lett.* **104** 057002 (2010).
- ¹² J. Zhao, D. T. Adroja, D.-X. Yao, R. Bewley, S. Li, X. F. Wang, G. Wu, X.-H. Chen, J. Hu, and P. Dai, *Nature Physics* **5** 555 (2009).
- ¹³ R. A. Ewings, T. G. Perring, J. Gillett, S. D. Das, S. E. Sebastian, A. E. Taylor, T. Guidi, and A. T. Boothroyd, *Phys. Rev. B* **83** 214519 (2011).
- ¹⁴ L. W. Harriger, H. Q. Luo, M. S. Liu, C. Frost, J. P. Hu, M. R. Norman, and P. Dai, *Phys. Rev. B* **84** 054544 (2011).
- ¹⁵ W. Ratcliff, P. A. Kienzle, J. W. Lynn, S. Li, P. Dai, G. F. Chen, and N. L. Wang, *Phys. Rev. B* **81** 140502 (2010).
- ¹⁶ M. Nakajima, S. Ishida, K. Kihou, Y. Tomioka, T. Ito, Y. Yoshida, C. H. Lee, H. Kito, A. Iyo, H. Eisaki, K. M. Kojima, and S. Uchida, *Phys. Rev. B* **81** 104528 (2010).
- ¹⁷ M. Rotter, M. Tegel, D. Johrendt, I. Schellenberg, W. Hermes, and R. Pöttgen, *Phys. Rev. B* **78** 020503 (2008).
- ¹⁸ S. Shamoto, M. Sato, J. M. Tranquada, B. J. Sternlieb, and G. Shirane, *Phys. Rev. B* **48** 13817 (1993).
- ¹⁹ J. Zhao, W. Ratcliff, J. W. Lynn, G. F. Chen, J. L. Luo, N. L. Wang, J. Hu, and P. Dai, *Phys. Rev. B* **78** 140504 (2008).
- ²⁰ Q. Huang, Y. Qiu, W. Bao, M. A. Green, J. W. Lynn, Y. C. Gasparovic, T. Wu, G. Wu, and X. H. Chen, *Phys. Rev. Lett.* **101** 257003 (2008).
- ²¹ A. I. Goldman, D. N. Argyriou, B. Ouladdiaf, T. Chatterji, A. Kreyssig, S. Nandi, N. Ni, S. L. Bud'ko, P. C. Canfield, R. J. McQueeney, *Phys. Rev. B* **78** 100506 (2008).
- ²² A. J. Freeman, *Acta Crystallogr.* **12** 261 (1959).
- ²³ A. J. Freeman, *Phys. Rev.* **113** 169 (1959).
- ²⁴ R. E. Watson and A. J. Freeman, *Acta Crystallogr.* **14** 27 (1961).

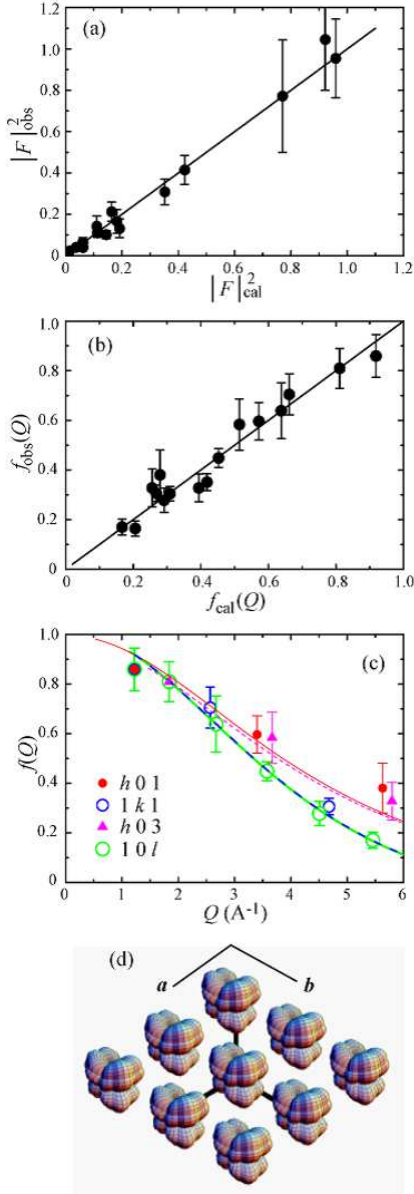


FIG. 4: (Color online) $|F|_{obs}^2$ (a) and $f_{obs}(Q)$ (b) are plotted against $|F|_{cal}^2$ and $f_{cal}(Q)$, respectively. Straight lines show $|F|_{obs}^2 = |F|_{cal}^2$ and $f_{obs}(Q) = f_{cal}(Q)$. (c) The $f_{obs}(Q)$ obtained at $h01$ (closed circles), $1k1$ (small open circles), $h03$ (closed triangles) and $10l$ (large open circles) reflections are plotted against Q . Thin solid and dashed lines are the magnetic form factors calculated at $h01$ and $h03$, bold dashed and solid lines are the magnetic form factors calculated at $1k1$ and $10l$, respectively. The bold dashed line corresponds with the bold solid lines. (d) Spin density of Fe ions in the orthorhombic unit cell is schematically shown in a - b plane.